Eur. Phys. J. B **33**, 365–372 (2003)
DOI: 10.1140/epjb/e2003-00177-4

THE EUROPEAN PHYSICAL JOURNAL B

AC Stark effect in toroidal carbon nanotubes threaded with an ac magnetic flux

Hong-Kang Zhao[a]

CCAST (World Lab.), PO Box 8730, Beijing 100080, PR China
and
Department of Physics, Beijing Institute of Technology, Beijing 100081, PR China

Received 20 November 2002 / Received in final form 7 February 2003
Published online 20 June 2003 –

Abstract. The ac Stark effect is investigated in the toroidal carbon nanotube system threaded with an ac magnetic flux. The Floquet theory is employed to deal with the time-dependent quantum problems. The time-averaged energy of the system is derived and is found to exhibit a strong relationship with an external field, and the modified energy gap has been presented. The ac flux enhances energy gaps to cause metal-semiconductor transition. The steady current has been obtained by employing the free energy approach, and the persistent current is a special case as the magnitude of the ac flux approaches zero. The photon-assisted current is quite different from the persistent current due to the absorption and emission of photons. The local density of states is obtained by calculating the Green's function in the Floquet state, and photon-resonant structures are observed. All of the novel features are associated with the ac Stark effect, which is caused by the modification of energy levels.

PACS. 73.63.Fg Nanotubes – 73.61.Wp Fullerenes and related materials – 73.22.-f Electronic structure of nanoscale materials: clusters, nanoparticles, nanotubes, and nanocrystals

1 Introduction

An important situation is that an electron is bound in an atom and placed in a weak uniform external electric field **E**. The field can be derived from an electrostatic potential $\phi(\mathbf{r}) = -\mathbf{E}.\mathbf{r}$, where the coordinate origin is most conveniently chosen at the position of the nucleus. In this system, the shift of the energy level in an electric field is known as the Stark effect [1]. For a homogeneous electric field applied to a periodic potential crystal system, the Bloch functions are modified as there is no interband coupling, and an electron in the crystal will move within one band with its wave vector **k** varying with time. Therefore, this leads to Wannier-Stark quantized energy levels $\varepsilon + n\alpha F$ $(n = 0, \pm 1, \pm 2, ...)$ deviating from the original one ε, where α is the lattice constant, and F is the magnitude of force on the electron due to the external field [2]. This level shifting was demonstrated experimentally by Koss and Lambert through observing the optical absorption of GaAs in a strong electric field [3]. When a magnetic field is applied to a large cylindrical molecule, such as a nanotube, field-induced level crossing takes place, and a linear Stark effect occurs, or the difference in quadratic Stark coefficient of two levels leads to a discontinuity in the polarization [4]. At sufficiently high external electromagnetic fields, such as in strong laser beams, the spectral structure of a small system can be modified drastically. The ac Stark effect plays an important role in causing multiphoton resonances. The observation of resonances in the photon-electron spectrum from the multiphoton ionization of xenon confirmed the fact. The investigation of ac Stark effects can help us understand the ionization dynamics [5–7]. The ac stark effect can shift initially nonresonant minibands in semiconductor superlattices into multiphoton resonance [8], and the photon-assisted mesoscopic tunneling is also associated with this effect [9,10].

Recently, many techniques have been developed to fabricate different structures of carbon nanotube (CN).The single-wall carbon nanotubes (SWCNs) are constructed by rolling up the graphite sheet in cylindrical form. The graphite sheet is composed of carbon with two inequivalent atoms forming an oriented honeycomb lattice. Each A atom is surrounded by three B atoms. Because of the variety geometrical and internal electron structures, CNs are found to have very unique transport and electronic features, such as the two facets of metallic and semiconducting behavior depending on their geometric aspects [11]. Since the experimental realization of a CN was performed by Iijima [12] in 1991, this field has attracted much attention both experimentally and theoretically. It opens up a new artificial laboratory to study one-dimensional transport [13–17] which is extensively investigated in

[a] e-mail: zhaohonk@yahoo.com

semiconductor quantum wire and hybrid device structures. The toroidal carbon nanotube (TCN) is a form of carbon structure, which is a torus structure by bending the carbon tube such that the two edges are connected. The tori proposed are constructed by introducing a single pentagon-heptagon pair into the perfect hexagon bonding pattern to connect carbon tubules [18]. In reference [19], the construction was based on the C_{60}, and the local topological structures of positive and negative Gaussian curvature were obtained theoretically. Haddon provided a theoretical investigation of the electron properties of TCN C_{576}, and revealed the quantum nature of a quasi-one-dimensional ring [20]. Martel *et al.* have fabricated rings from SWCNs, and they have observed magnetoresistance at low temperature [21]. The persistent current in TCNs was investigated and found to exhibit novel properties due to the modification of the energy structure and energy gap of the TCN by applying a magnetic field [22].

TCNs can be employed as functional electronic devices, such as switching and interference devices. The conductance of such a device can be controlled by adjusting the magnetic flux through the TCN since its energy gap is strongly associated with the magnetic flux. Usually, an electronic device is applied with an electromagnetic field, especially the radio frequency field. Therefore, it is interesting to consider the electronic properties induced by the electromagnetic field. The ac Stark effect plays a major role in such systems because the energy spectra are modified by the ac field. Correspondingly, the energy gaps and transport behavior are quite different from the dc field applied systems. In this paper, we investigate the physical properties of a TCN threaded with an ac magnetic flux. We suppose that electrons in the TCN are affected by the homogeneous vector potential. We use the Floquet theory to deal with the time-dependent quantum problems by casting the wave function into the extended Hilbert space. The time-averaged energy of the system has been derived, and the modified energy gap has been presented to compare with the one when the system is threaded with a dc flux. As the system is applied with a magnetic flux, the electrons in the TCN are driven by the field to form a current. This kind of current is caused by the interference behavior of electrons in the ring. We calculate the steady current of the system by employing the free energy approach, since the system can be taken as the pseudo-equilibrium state in the sense of quantum statistical mechanics. The persistent current is a special result as the magnitude of ac flux approaches zero. The multi-photon assisted current is quite different from the persistent current, since the absorption and emission of photons cause novel conducting behavior. The local density of states (LDOS) is obtained by calculating the Green's function of the system in the Floquet state, and photon-resonant structures are observed. In Section 2 we introduce our system and the Floquet theory briefly. The total energy and energy gap of the system are derived. Section 3 is devoted to the calculation of the steady state current from a statistical mechanics method. The multi-photon assisted steady current and persistent current are displayed there. We arrange the LDOS in Section 4, where the definition of the Green's function and the numerical results are given. The conclusion and summary are given in Section 5.

2 System formalism and energy levels

A TCN is formed by rolling a finite graphite sheet from the origin to the vectors $\mathbf{R}_{\rm x} = {\rm m}_1\mathbf{a}_1 + {\rm m}_2\mathbf{a}_2$, and $\mathbf{R}_{\mathbf{y}} = {\rm p}_1\mathbf{a}_1 + {\rm p}_2\mathbf{a}_2$ simultaneously. This indicates that the TCN satisfies the periodic boundary conditions along both of the longitudinal and transverse directions. In the $(\mathbf{e}_{\rm x}, \mathbf{e}_{\rm y}, \mathbf{e}_{\rm z})$ coordinates, the two-dimensional graphite sheet can be represented as a hexagonal lattice where the primitive lattice vectors of the graphite $\mathbf{a}_1$ and $\mathbf{a}_2$ are defined as $\mathbf{a}_1 = (3^{1/2}a/2, -a/2, 0)$ and $\mathbf{a}_2 = (3^{1/2}a/2, a/2, 0)$. The two primitive lattice vectors possess the same magnitude as $a = \mid \mathbf{a}_1 \mid = \mid \mathbf{a}_2 \mid = b \times 3^{1/2}$, where $b = 1.44$ Å is the C-C bond length of CNs known to be slightly larger than that of graphite [11]. We denote the TCNs by the convention $(m_1, m_2; p_1, p_2)$ [22,23]. In this paper, we focus on the highly symmetric armchair $(m, m; -p, p)$ TCN with an armchair structure along the transverse direction $\mathbf{e}_{\rm x}$, and a zigzag structure along the longitudinal direction $\mathbf{e}_{\rm y}$. In the rotating coordinate system with the base vectors $(\mathbf{e}_{\rm r}, \mathbf{e}_\theta, \mathbf{e}_{\rm z})$, the axis of the TCN is parallel to $\mathbf{e}_{\rm z}$. A time-dependent magnetic flux $\tilde{\phi}(t) = \phi + \phi_1 \sin(\omega t)$ is threaded through the TCN, where ϕ is a time-independent magnetic flux, ϕ_1 is the magnitude of the ac flux component, and ω is the angular frequency. Here we suppose that the ac flux is induced by the specially homogeneous electromagnetic vector potential $\mathbf{A}({\rm t})$ in the $\mathbf{e}_\theta$ direction, *i.e.*, $\mathbf{A}({\rm t}) = ({\rm A_r}, {\rm A}_\theta, {\rm A_z}) = (0, {\rm A}_\theta, 0)$, with $A_\theta = A_0 + A_\omega \sin(\omega t)$. For this vector potential we can find the magnetic field associated with the radial distribution as $\mathbf{B} = {\rm A}_\theta({\rm t})\mathbf{e}_{\rm z}/{\rm r}$ by $\mathbf{B} = \bigtriangledown \times \mathbf{A}({\rm t})$, where r is the distance of the field point from the z-axis. The electrical field is given by $\mathbf{E} = -\partial\mathbf{A}({\rm t})/\partial{\rm t}$, which has the form of $\mathbf{E} = -{\rm A}_\omega\omega\cos(\omega{\rm t})\mathbf{e}_\theta$. The vector potential produces the ac magnetic flux $\tilde{\phi}(t) = \oint \mathbf{A}({\rm t}) \cdot {\rm d}\mathbf{w}$, where $\mathbf{w}$ is the integral contour vector along the mesoscopic ring in the direction $\mathbf{e}_\theta$. We obtain the ac magnetic flux $\tilde{\phi}(t)$ with the dc magnetic flux magnitude $\phi = \pi D_t A_0$, and ac flux magnitude $\phi_1 = \pi D_t A_\omega$, where D_t is the diameter of the mesoscopic ring. This is a time-dependent periodic system with the period $T = 2\pi/\omega$, and it can be described by the time-dependent Hamiltonian $H(t) = H(t + T)$. By introducing the Floquet functions $u_{\mathbf{k}}(\mathbf{r}, {\rm t}) = \varphi_{\mathbf{k}}(\mathbf{r}) \exp\{-\frac{\rm i}{\hbar}\int_0^{\rm t}[{\rm E}[\mathbf{q}(\tau)] - \varepsilon(\mathbf{k})]{\rm d}\tau\}$, the time-dependent Schrödinger equation can be cast in the pseudo-equilibrium eigenvalue equation [8,24,25]

$$\hat{L}(t)u_{\mathbf{k}}(\mathbf{r}, {\rm t}) = \varepsilon(\mathbf{k}){\rm u}_{\mathbf{k}}(\mathbf{r}, {\rm t}), \tag{1}$$

where $\hat{L}(t) = H(t) - {\rm i}\hbar\frac{\partial}{\partial t}$, and $\varepsilon(\mathbf{k})$ is the energy of the Floquet state $u_{\mathbf{k}}(\mathbf{r}, {\rm t})$ given by

$$\varepsilon(\mathbf{k}) = \frac{1}{\rm T}\int_0^{\rm T} {\rm d}\tau {\rm E}[\mathbf{q}(\tau)], \tag{2}$$

with $\mathbf{q}(\mathrm{t}) = \mathbf{k} - \mathrm{e}\mathbf{A}(\mathrm{t})/\hbar$. $E(\mathbf{k})$ is the energy level with the eigenfunction $\varphi_{\mathbf{k}}(\mathbf{r})$ of the system in the absence of an external magnetic field $\mathbf{A}(\mathrm{t})$. Due to the gauge transformation, the time-dependent energy is given by replacing $\mathbf{k}$ by $\mathbf{q}(\mathrm{t})$. The periodic boundary conditions lead to the situation that the Brillouin-zone edge oscillates with time [26]. In the Floquet theory, the Hilbert space has to be extended by defining the extended states $\Psi_{\mathbf{k},\mathrm{n}}(t) = u_{\mathbf{k}}(\mathbf{r},\mathrm{t})\exp(\mathrm{in}\omega\mathrm{t})$ as the base of the Hilbert space. In this situation, the energy possesses side-bands associated with the absorption and emission of n photons as $\tilde{E}_n(\mathbf{k}) = \varepsilon(\mathbf{k}) + \mathrm{n}\hbar\omega$, $(n = 0, \pm1, \pm2, ...)$. This means that $\hat{L}(t)\Psi_{\mathbf{k},\mathrm{n}}(t) = \tilde{E}_n(\mathbf{k})\Psi_{\mathbf{k},\mathrm{n}}(\mathrm{t})$, which defines the multiple photon-assisted pseudo-equilibrium state. The wavefunction of the system is a linear combination of the extended Floquet state $\Psi(\mathbf{r},\mathrm{t}) = \sum_{\mathrm{n}\mathbf{k}} \mathrm{C}_{\mathbf{k}}\mathrm{J}_{\mathrm{n}}(\alpha_1)\Psi_{\mathbf{k},\mathrm{n}}(\mathrm{t})$, where $C_{\mathbf{k}}$ is the annihilation operator of the electron, $J_n(\alpha)$ are the Bessel functions of the first kind.

The diameter d_t of tube is determined by $d_t = 3bm/\pi$, while the diameter of the ring is determined by $D_t = 3^{1/2}bp/\pi$. The ratio of the two diameters $\kappa = d_t/D_t = 3^{1/2}m/p$. The electron energy structure and transport property of this TCN system are mainly determined by the π valence electrons. Tight-binding calculations for the π electrons are proved to be in good agreement with experiment. They can provide important insights for understanding the electron structure of the π energy level in the CNs system. In the absence of an external electromagnetic field, the energy dispersion is degenerate at the K point in the Brillouin zone [11]. However, as the external electromagnetic field is applied to the system, the energy spectrum is modified considerably by the dc and ac components of the applied field. The periodic boundary condition of a TCN requires that $\mathbf{q}(\mathrm{t})$ must satisfy the relation $q_x = 2\pi j/3bm$, and $q_y = 2\pi[\ell + \tilde{\phi}(t)/\phi_0]/3^{1/2}bp$, where $\phi_0 = h/e$ is the flux quantum, $(j = 1, 2, ..., m; \ell = 1, 2, ..., 2p)$. The energy of this TCN system is quantized in the longitudinal and transversal directions, and the energy also shifts to exhibit an ac Stark effect, *i.e.*, the discrete energy $\tilde{E}_{\ell j,n\delta}(\phi,\phi_1) = \varepsilon_{\ell j,\delta}(\phi,\phi_1) + n\hbar\omega$, $(n = 0, \pm1, \pm2, ...)$. This signifies that each π and π^* energy level is shifted due to the valence electrons absorbing and emitting photons. In this paper, we treat the TCN with the ratio of two diameters $\kappa \ll 1$, which signifies that the inner structure of the nanotubes does not enter our treatment. Furthermore, we make an approximation by neglecting the coupling between different bands, and only consider the photon absorption and emission procedures. The tight-binding calculation reveals that this armchair TCN energy is given by

$$\varepsilon_{\ell j,\delta}(\phi,\phi_1) = \delta\gamma_0\Bigg\{1 + 4\sum_{n=-\infty}^{\infty}\left[J_{2n}^2(\alpha_1)\cos^2(\beta_\ell) + J_{2n+1}^2(\alpha_1)\sin^2(\beta_\ell)\right] + 4J_0(\alpha_1)\cos(\beta_\ell)\cos\left(\frac{j\pi}{m}\right)\Bigg\}^{1/2}, \quad (3)$$

where $\beta_\ell = \pi(\ell + \phi/\phi_0)/p$, $\alpha_1 = \pi\phi_1/p\phi_0$, $j = 1, 2, ..., m; \ell = 1, 2, ..., 2p; \delta = \pm$, and $\gamma_0 = 3.033$ eV. The upper half of the energy dispersion curves describes the π^*-energy anti-bonding band (unoccupied state), and the lower half of it is the π-energy bonding band (occupied state). Defining $\Omega = \phi_0/3^{1/2}\pi b = 5.3 \times 10^{-4}$ T m, the dimensionless quantity α_1 can be expressed as $\alpha_1 = A_\omega/\Omega$. The energy is a periodic function of ϕ with period ϕ_0, and its magnitude relies on the magnitude of the ac field. By varying A_ω continuously, the energy varies accordingly and passes through the zeros of $J_n(\alpha)$, and some novel behavior will be observed. From the energy of the TCN, we find that the ac Stark effect not only shifts the electron level by $n\hbar\omega$, but it also modifies the magnitude of the original electron energy levels. Since the Bessel functions $J_n(\alpha)$ possess the property at $\alpha = 0$, $J_0(0) = 1$, and $J_n(0) = 0$ for $n \neq 0$, the energy given above reduces to the energy dispersion of an armchair TCN as $A_\omega \to 0$ [22]. Due to the modification of the energy dispersion, the metallic TCN changes to a semiconductor according to the modification of the energy gap. On the other hand, even if the system is semiconducting, the valence electrons can become conducting electrons by absorbing enough photon energy, and the conducting electrons become valence electrons by emitting enough photons. This effect can be employed to contrive photon-electron TCN devices.

The straight armchair CN with the indices (m, m) is always metallic in the absence of an external field. But for the metallic armchair $(m, m; -p, p)$ TCN, it requires that p be a multiple of 3 which is referred to as a type I TCN), *i.e.*, $p = 3\nu$, where ν is an integer. The highest occupied state and the lowest unoccupied state meet with each other at the Fermi energy E_F in the absence of an external magnetic field. Due to the symmetric structure, the Fermi energy is located at $E_F = 0$. The semiconductor armchair TCN in the absence of an external field requires the index p satisfy the relation $p = 3\nu \pm 1$ (which is referred to as a type II TCN). The energy gap is determined by the electron state as $j = m$, and $\ell = \nu, \nu - 1$. However, as the external electromagnetic field is applied to the TCN, the energy gap changes, and it is intimately related to the magnitude of the field. The energy gap of the armchair TCN in the presence of an electromagnetic field is modified now being associated with the form

$$E_g^{(\mp)}(\phi,\phi_1) = 2\gamma_0\Bigg\{3 - \left[1 - 2\sum_{n=-\infty}^{\infty}J_{2n+1}^2(\alpha_1)\right]z^{(\pm)}(2\xi) - 2J_0(\alpha_1)z^{(\mp)}(\xi)\Bigg\}^{1/2}, \quad (4)$$

where $z^{(\pm)}(\xi) = \cos(\xi) \pm 3^{1/2}\sin(\xi)$. The side-band energy shift is not included in the energy gap formula above, which we will discuss later. The energy gap formula is different for different types of CN and magnetic flux regions. For the type I armchair TCN, the energy gap $E_g(\phi,\phi_1)$ is determined by $E_g(\phi,\phi_1) = E_g^{(+)}(\phi,\phi_1)$, with $\xi = \chi_0\phi/\phi_0$ in the region $0 \leq \phi \leq \phi_0/2$, which is related to the

energy state $j = m, \ell = \nu$. R is the radius of ring, and $\chi_0 = 3^{1/2}b/2R$. In the region $\phi_0/2 \leq \phi \leq \phi_0$, it is determined by $E_g(\phi, \phi_1) = E_g^{(-)}(\phi, \phi_1)$, with $\xi = \chi_0(1 - \phi/\phi_0)$ associated with the state $j = m, \ell = \nu - 1$. For the type II armchair TCN, the energy gap is determined by $E_g(\phi, \phi_1) = E_g^{(-)}(\phi, \phi_1)$ with $\xi = \chi_0(1/3 - \phi/\phi_0)$ in the region $0 \leq \phi \leq \phi_0/2$, which is associated with the state $j = m, \ell = \nu$. In the region $\phi_0/2 \leq \phi \leq \phi_0$, it is determined by $E_g(\phi, \phi_1) = E_g^{(-)}(\phi, \phi_1)$,with $\xi = \chi_0(2/3 - \phi/\phi_0)$, which is associated with the state $j = m, \ell = \nu - 1$. For the type I TCN as $\phi = 0, \phi_0$, and for the type II TCN as $\phi = \phi_0/3$, $2\phi_0/3$, respectively, the energy gap shown in equation (4) is reduced to

$$E_g(\phi_1) = 2 \times 2^{1/2}\gamma_0 \left[1 - J_0(\alpha_1) + \sum_{n=-\infty}^{\infty} J_{2n+1}^2(\alpha_1)\right]^{1/2}. \quad (5)$$

Obviously, as $\alpha_1 \to 0$, the energy gaps disappear at these points. The TCNs can exhibit metallic behavior even if they are semiconducting TCNs in the absence of an external field. The ac flux modifies these zero energy gaps to nonzero ones. This signifies that the dc flux modifies the conducting properties of TCNs from semiconductor to metal transition at these points, while the ac flux increases the energy gaps to form semiconducting TCNs with large gaps. The energy gaps increase tremendously with increasing magnitude α_1. In the absence of an external ac field, *i.e.*, $\alpha_1 = 0$, equation (4) is reduced to $E_g^{(\pm)}(\phi) = 2\gamma_0 \mid 1 - z^{(\pm)}(\xi) \mid$, with ξ given above in different regions of ϕ. If the radius R is very large such that $\chi_0 \ll 1$, the energy gap is then given by the one shown in reference [22]. For a type I armchair TCN, $E_g(\phi) = \Delta_0\phi/\phi_0$ as $0 \leq \phi \leq \phi_0/2$; $E_g(\phi) = \Delta_0(1 - \phi/\phi_0)$ as $\phi_0/2 \leq \phi \leq \phi_0$, where $\Delta_0 = 3b\gamma_0/R$. For a type II armchair TCN, $E_g = \Delta_0 \mid 1/3 - \phi/\phi_0 \mid$ in the region $0 \leq \phi \leq \phi_0/2$; $E_g(\phi) = \Delta_0 \mid 2/3 - \phi/\phi_0 \mid$ in the region $\phi_0/2 \leq \phi \leq \phi_0$.

We have examined that there is no major difference in the physical properties for the rings: (1) type I $(10, 10; -5001, 5001)$ and $(10, 10; -480, 480)$ TCNs; (2) type II $(10, 10; -5002, 5002)$ and $(10, 10; -481, 481)$ TCNs. This signifies that our results discussed so far possess a common feature of the system if the ring is large enough. To illustrate the corresponding behavior of the energy structure and pseudo-equilibrium properties, we perform the investigation of two samples: (a) the type I $(10, 10; -480, 480)$ TCN ;(b) the type II $(10, 10; -481, 481)$ TCN. For these TCNs, the index p satisfies $p = 3\nu$, and $p = 3\nu + 1$ with $\nu = 160$. For the type I $(10, 10; -480, 480)$ TCN, the diameter of the tube $d_t = 13.75$ Å, and the diameter of the ring $D_t = 381.10$ Å. The ratio of the two diameters is $\kappa \approx 0.036$. For the type II $(10, 10; -481, 481)$ TCN, the diameter d_t is the same as the former one, but the diameter $D_t = 381.89$ Å. The diameter ratio is $\kappa \approx 0.036$. Figure 1 shows the energy levels of $(10, 10; -480, 480)$ TCN in the presence of the ac flux at $\phi = 0$. The upper half energy levels exhibit the π^*-energy anti-bonding band variation with the magnitude of the ac flux, while the lower half energy levels represent the π-energy bonding band displaying the symmetric modification compared with the upper one. At $\alpha_1 = 0$, the lowest π^*-energy anti-bonding level and the highest π-energy bonding level meet each other. This signifies that the energy gap is zero at this point. As α_1 increases, the two energy bands separate to form a large energy gap, and it does not disappear for $\alpha_1 \neq 0$. Each of the two energy levels bends up and down, and then the energy levels knit together by increasing the magnitude of the ac flux. The knitting points of the energy bands are associated with the zeros of the Bessel functions. The modification of the energy bands due to an ac flux is a kind of ac Stark effect. Since an ac Stark effect in this system increases the energy gap to change the metallic armchair TCN into a semiconducting one, the behavior of electrons in this system is quite different from the one without applying the ac flux. One observes that the energy gap is very large if the ac flux is strong enough. The first knitting point is located at $\alpha_1 = 2.2$ which is related to the magnitude of the ac magnetic field $B_1 = 6.12 \times 10^4$ T on the ring by $B_1 = A_\omega/R$.

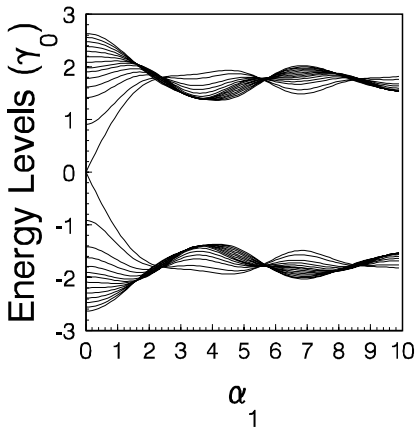

Fig. 1. The energy levels of the $(10, 10; -480, 480)$ TCN *versus* α_1 for the case when the dc magnetic flux $\phi = 0$. The energy shift by absorbing and emitting photons is not displayed.

We present the energy gap with respect to the magnetic flux ϕ in Figure 2. Diagrams (a) and (b) correspond to the situations in the absence ($\alpha_1 = 0$), and in the presence ($\alpha_1 \neq 0$) of an ac magnetic flux component, respectively. In diagram (a), the solid and dotted curves are associated with the energy gaps of $(10, 10; -480, 480)$ and $(10, 10; -481, 481)$ TCNs. As the dc flux is zero, the $(10, 10; -480, 480)$ TCN is metallic, while the $(10, 10; -481, 481)$ TCN is semiconducting with a small energy gap. The energy gaps change periodically by increasing the flux ϕ. This means that the TCNs show metallic and semiconducting properties periodically with ϕ. The metal-semiconductor transition induced by the magnetic flux was predicted in a straight infinite CN [27], and in large TCNs [22], where the transitions occur periodically at points. This means that at some points of ϕ the TCN behaves like a metal, while at other points the TCN behaves like a semiconductor. For

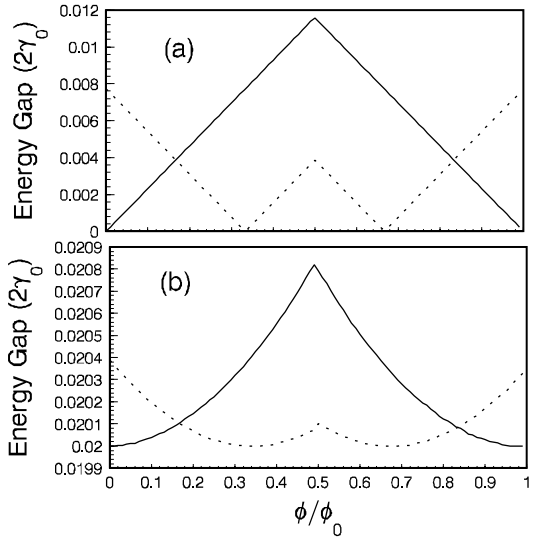

Fig. 2. The energy gap E_g of the TCN *versus* dc magnetic flux ϕ. Diagram (a) shows the case for $\alpha_1 = 0$. The solid curve is associated with the $(10, 10; -480, 480)$ TCN, while the dotted curve is related to the $(10, 10; -481, 481)$ TCN. Diagram (b) shows the case for $\alpha_1 = 0.02$. The solid curve is associated with the $(10, 10; -480, 480)$ TCN, while the dotted curve is related to the $(10, 10; -481, 481)$ TCN.

a type I TCN, the metal-semiconductor transition points in a period are located at $\phi = 0, \phi = \phi_0$, while for the type II TCN, the metal-semiconductor transition points in a period are located at $\phi = \phi_0/3, 2\phi_0/3$. The magnitudes of the dc magnetic field on the ring corresponding to the above transition points are $B_0 = 0, 1.814$ T, for the type I TCN, and for the type II TCN $B_0 = 0.605, 1.209$ T, respectively. This behavior is modified by applying the ac flux to the TCNs shown in diagram (b). First, there is no metallic property in the systems at $\alpha_1 = 0.02$. The corresponding ac magnetic amplitude on the ring is $B_1 = 5.56 \times 10^2$ T. The TCNs are always semiconducting no matter what the dc flux ϕ is. Second, the shapes and magnitudes of the energy gap vary periodically with some modifications compared with the ones without an ac flux. The maximum and minimum energy gaps are dominated by the magnitude of the ac flux α_1. The period of the energy gap is ϕ_0, which is the same period as the system for $\alpha_1 = 0$. Type I and type II TCNs possess quite different energy gaps. The energy gap can reach a very large value $E_g \sim 2.8\gamma_0$ for $\alpha_1 > 1.4$, which can be seen from Figure 1 by comparing the energy levels.

3 Steady state current

The persistent current is an equilibrium property of a mesoscopic ring which can be derived from the free energy of the system. However, time-dependent system disturbed by an ac flux is in a nonequilibrium state. Since the Floquet state can describe the pseudo-equilibrium state, we can therefore expand the time-dependent nonequilibrium state as the combination of pseudo-equilibrium states. Because the statistical mechanics determines physical behaviors by taking a time average and an ensemble average, we can also obtain the free energy of the system applied with a time-dependent magnetic flux. The time-averaged TCN free energy is given by

$$F(\phi, \phi_1) = -k_B T \sum_{\ell j n \delta} J_n^2(\alpha_1) \times \ln\{1 + \exp[-(\tilde{E}_{\ln j, n\delta}(\phi, \phi_1) - E_F)/k_B T]\}, \quad (6)$$

where T is the temperature of the system, k_B the Boltzmann constant, and $\tilde{E}_{\ell j, n\delta} = \varepsilon_{\ell j, \delta} + n\hbar\omega$ is the energy level with $\varepsilon_{\ell j, \delta}$ defined in equation (3). The free energy is weighted by $J_n^2(\alpha_1)$ which declines with increasing n. This signifies that the probability of the absorbing and emitting of a photon procedure decreases with increasing photon number. In principle, the system can be assisted with an infinite number of photons. In practice we only need to consider a low order of photon-assisted procedure since the contribution of higher numbers of photons is quite small. From this free energy, we can derive the steady state current by taking the derivative over the flux ϕ, *i.e.*, $I = -\partial F(\phi, \phi_1)/\partial\phi$. This current is a time-averaged one which can be measured experimently. Obviously, as $\alpha_1 \to 0$, the free energy reduces to the one in the absence of the ac magnetic flux, and the steady state current is a persistent current. The steady state current is obtained straightforwardly by taking the partial derivative of the free energy (6) with respect to ϕ, which is formulated as

$$I(\phi, \phi_1) = I_0\gamma_0 \sum_{\ell j n \delta} \frac{\Gamma_{\ell j}(\phi, \phi_1)}{\varepsilon_{\ell j, \delta}(\phi, \phi_1)} J_n^2(\alpha_1) f[\tilde{E}_{\ell j, n\delta}(\phi, \phi_1)] \sin(\beta_\ell), \quad (7)$$

where

$$\Gamma_{\ell j}(\phi, \phi_1) = J_0(\alpha_1) \cos\left(\frac{j\pi}{m}\right) + 2\cos(\beta_\ell) \left[1 - 2 \sum_{n=-\infty}^{\infty} J_{2n+1}^2(\alpha_1)\right],$$

and $I_0 = 4\pi\gamma_0/p\Phi_0$. In the current formula above, $f(\epsilon)$ is the Fermi-Dirac distribution function. The magnitude of the steady current is dependent on the index p, and it is strongly associated with the magnitude of the ac flux. The current is inversely proportional to p, which means that as $p \to \infty$, the current disappears. Since the ac flux increases the energy gap, one can expect that the steady current is suppressed extensively by the ac flux.

We display the persistent current of $(10, 10; -480, 480)$ and $(10, 10; -481, 481)$ TCNs in Figure 3a at zero temperature. The current is scaled by $I_0 = 3 \times 10^{-6}$ A for these systems. The persistent current is carried in the whole π-band channels and the lowest π^*-band channel although different channels carry different portions of current. As a result, some of current parts are cancelled, and the net current is sensitive to the types of TCN. The current oscillates periodically with a period ϕ_0, and it satisfies the

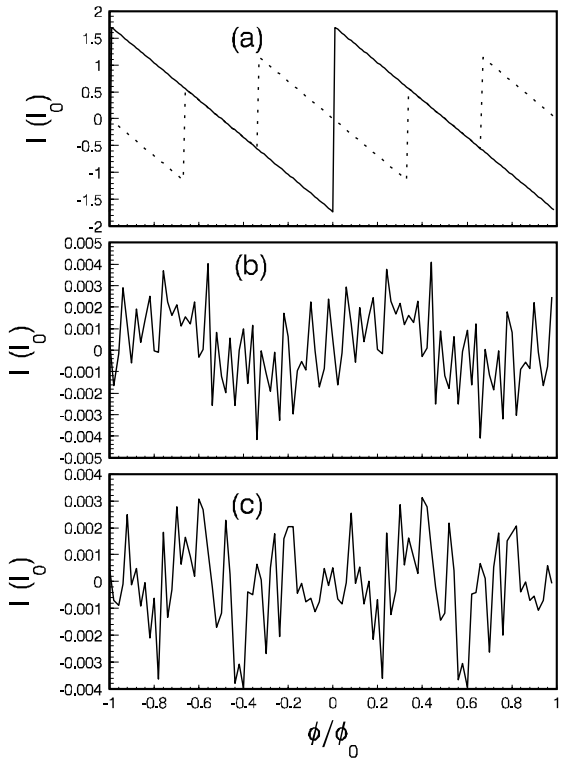

Fig. 3. The steady current *versus* dc magnetic flux ϕ. Diagram (a) shows the persistent current at $\alpha_1 = 0$. The solid curve corresponds to the $(10, 10; -480, 480)$ TCN, while the dotted curve is related to the $(10, 10; -481, 481)$ TCN. Diagrams (b) and (c) display the steady current of the $(10, 10; -480, 480)$ TCN and the $(10, 10; -481, 481)$ TCN, respectively, for $\alpha_1 = 0.05$ and $\hbar\omega/\gamma_0 = 0.01$.

symmetric property $I(\phi + \phi_0/2) = -I(-\phi + \phi_0/2)$, which means that in a period $0 \sim \phi_0$ the current is an odd function of ϕ at $\phi_0/2$ [28]. The current is zero if the static flux $\phi = 0$. In a period ϕ_0 the current of a type I TCN only oscillates once, while the current of a type II TCN oscillates twice. This behavior for different types of TCN is caused by the situation that the type I TCN possesses one metal-semiconductor transition, but the type II TCN possesses two metal-semiconductor transitions in a period. The type I TCN carries a larger persistent current than that of the type II TCN. The steady current *versus* ϕ in the presence of an ac flux at $\alpha_1 = 0.05$ is depicted in Figures 3b and c for $(10, 10; -480, 480)$ and $(10, 10; -481, 481)$ TCNs, respectively, where $\hbar\omega = 0.01\gamma_0$. The corresponding magnitude of the ac magnetic field required on the ring is $B_m = 1.39 \times 10^3$ T, and the frequency is 7.36×10^{12} Hz. One observes that the current oscillates with ϕ periodically with a period ϕ_0. However, in each period, the current vibrates fiercely. This behavior is somewhat like the situation where the persistent current carries high oscillating current. Compared with the persistent current, one observes that the steady current is strongly suppressed by the ac flux due to the increasing energy gap. The formation of a current can be understood as the physical procedure. The application of an ac flux results in the increasing of the energy gap of the system. Due to the symmetric

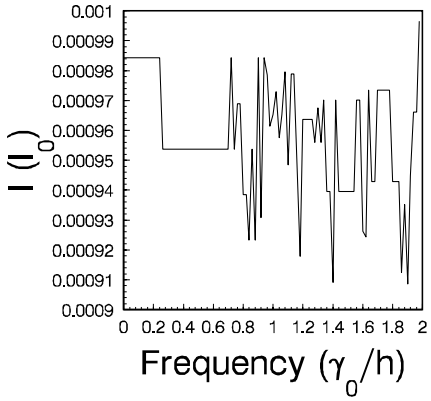

Fig. 4. The steady current for the $(10, 10; -480, 480)$ TCN *versus* the frequency of an ac flux. The parameters are chosen such that $\phi = 0, \alpha_1 = 0.02$, and the frequency is scaled by $\gamma_0/h = 7.36 \times 10^{14}$ Hz.

structures of TCNs, the Fermi level is located between the energy bands with $E_F = 0$. At zero temperature, a current is produced if the condition $\varepsilon_{\ell j,\delta}(\phi, \phi_1) + n\hbar\omega \leq E_F$ is satisfied. For the π-band, this condition is naturally satisfied in the absence of an ac flux. In the presence of an ac flux, the π-band shifts up and down due to absorbing and emitting photons. If the π-band absorbs photons to shift the energy band up as $\varepsilon_{\ell j,\delta}(\phi, \phi_1) + n\hbar\omega > E_F$ (where $n > 0$), then there is no current carried by the π-band. On the other hand, the π^*-band does not carry current in the absence of an ac flux except in the lowest energy level. However, in the presence of an ac flux, this band shifts down by emitting photons to meet $\varepsilon_{\ell j,\delta}(\phi, \phi_1) + n\hbar\omega \leq E_F$ (where $n < 0$), then this π^*-band can also carry current. The shift of the energy bands is the ac Stark effect. Therefore, the ac Stark effect results in the novel conducting properties in the TCNs. The conducting behavior is strongly associated with the type of TCN, which can be seen obviously from Figure 3.

The variation of the steady state current *versus* the frequency of the ac flux is presented in Figure 4 at $\phi = 0$, and $\alpha_1 = 0.02$. The corresponding magnitude of the ac magnetic field on the ring is $B_m = 5.56 \times 10^2$ T. The frequency is scaled by $\gamma_0/h = 7.36 \times 10^{14}$ Hz. As the frequency lies in the region $0 \sim 0.22\gamma_0/h$, the current is a constant $I = 9.84 \times 10^{-4} I_0$, and as the frequency lies in the region $0.22 \sim 0.64\gamma_0/h$, the current jumps to another value $I = 9.54 \times 10^{-4} I_0$. Then by increasing the frequency, the current oscillates fiercely to exhibit a sensitivity of current against frequency. The behavior of steady current *versus* frequency suggests that we can employ the TCN to make a switching device which is controlled by the frequency and magnitude of the ac flux.

4 Local density of states

The LDOS is a quantity that can be measured by scanning tunneling microscopy (STM). Recent STM studies of SWCNs have confirmed the electronic properties, such as the Van Hove singularities [29], by measuring the LDOS.

The LDOS can be defined by the imaginary part of a diagonal Green's function in the local representation. Due to the symmetric structure of the TCN system, the LDOS acts as the bulk density of states (DOS) since there is no edge effect. We perform the calculation of LDOS from the definition

$$\rho(\epsilon,\phi,\phi_1) = -\frac{1}{\pi}\mathrm{Im}G^r(\epsilon,\phi,\phi_1). \tag{8}$$

The Green's function $G^r(\epsilon,\phi,\phi_1)$ of the pseudo-equilibrium system can be obtained by applying the extended Floquet state to the quantum operator $\hat{L}(t)$ as the usual definition of Green's function [25]. For the diagonal elements of the local Green's function, we can express it by the photon-assisted energy shift as

$$G^r(\epsilon,\phi,\phi_1) = \frac{1}{N}\sum_{\ell mjs\delta}\frac{J_m^2(\alpha_1)\mid K_{s-m}^{\ell j}(\phi,\phi_1)\mid^2}{\epsilon-\tilde{E}_{\ell j,s\delta}(\phi,\phi_1)+\mathrm{i}\eta}, \tag{9}$$

where $K_n^{\ell j}(\phi,\phi_1)$ is the Fourier transformed version associated with time t through the equation

$$\sum_n K_n^{\ell j}(\phi,\phi_1)\mathrm{e}^{\mathrm{i}n\omega t} = \exp\left\{-\frac{\mathrm{i}}{\hbar}\int_0^t \mathrm{d}\tau[E_{\ell j,\delta}[\mathbf{q}(\tau)]-\varepsilon_{\ell\mathrm{j},\delta}(\phi,\phi_1)]\right\}.$$

N is the number of unit cells in the TCN, and $\eta\to+0$. For the $(m,m;-p,p)$ TCN system, the number of unit cells is equal to the index p, *i.e.*, $N=p$. By expanding the time-dependent energy levels near the energy $\varepsilon_{\ell j,\delta}(\phi,\phi_1)$, we can obtain the expression of $K_n^{\ell j}(\phi,\phi_1)$ approximately by keeping the leading orders to give

$$K_s^{\ell j}(\phi,\phi_1) = \sum_n J_n(\Lambda_{\ell j})J_{s-n}(\zeta_\ell),$$

where

$$\Lambda_{\ell j} = \frac{4\gamma_0}{\hbar\omega}J_1(\alpha_1)\cos(\beta_\ell)\cos(j\pi/m),$$
$$\zeta_\ell = \frac{4\gamma_0}{\hbar\omega}J_0(\alpha_1)J_1(\alpha_1)\cos(2\beta_\ell).$$

The LDOS therefore can be derived by substituting equation (9) into the definition given in equation (8). The expression of LDOS is very complicated due to the absorption and emission of photons, since the photon-assisted procedure is associated with the magnetic flux components ϕ and ϕ_1. The Green's function is weighted by $J_m^2(\alpha_1)$ and $\mid K_{s-m}^{\ell j}(\phi,\phi_1)\mid^2$. This signifies that the intensity of absorption and emission of photons is determined by the magnitudes of ϕ and ϕ_1. As $\alpha_1\to 0$, we have the Green's function of the system in the absence of the ac magnetic flux component.

We show the LDOS for $(10,10;-480,480)$ and $(10,10;-481,481)$ TCNs in the presence of an ac flux in Figures 5a and b, respectively. The frequency of the external field is in the microwave range at 7.36×10^{12} Hz.

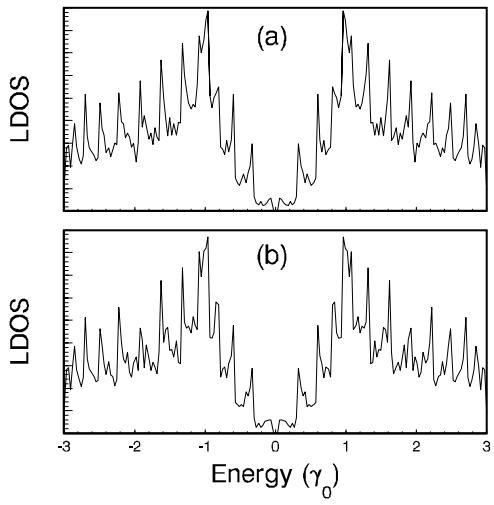

Fig. 5. LDOS of a TCN *versus* energy in the presence of an ac magnetic flux. The parameters are chosen such that $\hbar\omega = 0.01\gamma_0, \alpha_1 = 0.05, \phi = 0$. Diagrams (a) and (b) are associated with $(10,10;-480,480)$ and $(10,10;-481,481)$ TCNs, respectively. The parameters are chosen such that $\hbar\omega = 0.01\gamma_0, \alpha_1 = 0.05, \phi = 0$.

The magnitude of the ac flux is determined by $\alpha_1 = 0.05$, and the static flux is zero by setting $\phi = 0$. The corresponding magnitude of the ac magnetic field on the ring is $B_m = 1.39\times10^3$ T. The type I and type II TCNs exhibit small energy gaps about $E_g \sim 30$ meV. As the external magnetic flux is removed, the type I $(10,10;-480,480)$ TCN becomes a metal with zero energy gap $E_g = 0$, while type II $(10,10;-481,481)$ TCN becomes a semiconductor with the energy gap $E_g \approx 23$ meV shown in Figure 2a. This indicates that the ac flux enhances the energy gap to cause the metal-semiconductor transition. We also observe the resonant peaks obviously associated with photon absorption and emission. In the absence of an ac flux, the LDOS displays close resonant peaks related to discrete energy levels. Some of the peaks are suppressed while some of them are enhanced due to the photon absorption and emission effect. The compound process yields a novel electronic structure, and results in quite different conducting behavior which we have seen in Figure 3. The symmetric structure of the LDOS around $E = 0$ indicates that the topological symmetry of TCNs is not broken by introducing an ac flux. The LDOSs of type I and type II TCNs exhibit subtly different structures since the main behavior of system is dominated by the ac flux. However, this slight difference of LDOS implies a distinctly different transport behavior of the two systems, such as the steady current shown in Figure 3.

5 Concluding remarks

We have investigated the ac Stark effect in TCNs threaded through an ac magnetic flux. The modification of the energy levels is strongly dependent on the specific structures of the samples. For a sample system in the mesoscopic range, the interference takes effect, and electrons move coherently to form a persistent current. In the TCN system,

coherent behavior of electrons result in novel properties compared with usual metallic or semiconducting systems since their energy gaps are adjusted by an external magnetic flux. The metal-semiconductor transition induces a specific conducting current. The ac flux bends the energy levels up and down, and enhances the energy gap eventually. This causes the type I metallic TCN to be semiconducting, and the energy gap can be very large by increasing the magnitude of the ac flux. The current is formed due to two procedures. One is the persistent current as the static flux ϕ is applied to the system, and the other part is caused by the photon absorption and emission procedure. The compound effect is the composition of two components of current to produce an oscillating current which fluctuates fiercely with ϕ. The period of the current *versus* flux ϕ is the flux quantum ϕ_0, but the detailed oscillation structure is dependent on the frequency and structure of the TCN. The LDOS is given by calculating the imaginary part of the Green's function in the Floquet state. In the extended Hilbert space, the whole system is in a pseudo-equilibrium state. This causes us to employ quantum statistical mechanics to handle the photon-assisted system conveniently. Photon-resonant peaks are observed in LDOS due to the suppression and enhancement of some resonant peaks, which can be measured by STM. Since there are several external parameters such as static flux, magnitude and frequency of the ac flux, we can control the conducting behavior by adjusting the parameters. This leads us to contrive novel devices to meet different application purposes, such as switching and photon-electron devices. Since the modification of the energy levels has a major effect on the system, we conclude that the ac Stark effect plays an important role in the mesoscopic TCN system not only in fundamental phenomena, but also in technical applications.

This work was supported by the National Natural Science Foundation of China under the Grant No. 19875004, and by the fellowship under the Distinguished Visiting Scholar Program of the Chinese Government.

References

1. E. Merzbacher, *Quantum Mechanics* (New York, John Wiley and Sons, INC., 1961)
2. G.H. Wannier, Phys. Rev. **117**, 432 (1960); Rev. Mod. Phys. **34**, 645 (1962)
3. R.W. Koss, L.M. Lambert, Phys. Rev. B **5**, 1479 (1972)
4. P. Fulde, A. Ovchinnikov, Eur. Phys. J. B **17**, 623 (2000); S. Pleutin, A. Ovchinnikov, Eur. Phys. J. B **23**, 521 (2001); S. Pleutin, A. Ovchinnikov, Carbon **40**, 129 (2002)
5. R.R. Freeman *et al.*, Phys. Rev. Lett. **59**, 1092 (1987)
6. R.B. Vrijen, J.H. Hoogenraad, H.G. Muller, L.D. Noordam, Phys. Rev. Lett. **70**, 3016 (1993)
7. J.G. Story, D.I. Duncan, T.F. Gallagher, Phys. Rev. Lett. **70**, 3012 (1993)
8. M. Holthaus, D.W. Hone, Phys. Rev. B **49**, 16605 (1994)
9. P.S.S. Guimaraes *et al.*, Phys. Rev. Lett. **70**, 3792 (1993)
10. H.K. Zhao, Z. Phys. B **102**, 415 (1997); H.K. Zhao, G.v. Gehlen, Phys. Rev. B **58**, 13660 (1998); H.K. Zhao, J. Wang, Eur. Phys. J. B **9**, 513 (1999)
11. R. Saito, G. Dresselhaus, M.S. Dresselhaus, *Physical Properties of Carbon Nanotubes* (Imperial College Press, London, 1998)
12. S. Iijima, Nature (London) **354**, 56 (1991)
13. S.J. Tans, M.H. Devoret, H. Dai, A. Thess, R.E. Smalley, L.J. Geerligs, C. Dekker, Nature (London) **386**, 474 (1997); C. Zhou, J. Kong, H. Dai, Phys. Rev. Lett. **84**, 5604 (2000)
14. T.W. Odom, J.L. Huang, P. Kim, C.M. Lieber, Nature **391**, 62 (1998); S.J. Tans, A.R.M. Verschueren, C. Dekker, Nature **393**, 49 (1998)
15. A. Bachtold, C. Strunk, J.P. Salvetat, J.M. Bonard, L. Forró, T. Nussbaumer, C. Schönenberger, Nature **397**, 673 (1999)
16. W. Tian, S. Datta, Phys. Rev. B **49**, 5097 (1994); Y. Xue, S. Datta, Phys. Rev. Lett. **83**, 4844 (1999)
17. H. Mehrez, J. Taylor, H. Guo, J. Wang, C. Roland, Phys. Rev. Lett. **84**, 2682 (2000); C. Roland, M.B. Nardelli, J. Wang, H. Guo, Phys. Rev. Lett. **84**, 2921 (2000)
18. B.I. Dunlap, Phys. Rev. B **46**, 1933 (1992)
19. S. Itoh, S. Ihara, J. Kitakami, Phys. Rev. B **47**, 1703 (1993); *ibid.* **47**, 12908 (1993)
20. R.C. Haddon, Nature **388**, 31 (1997)
21. R. Martel, H.R. Shea, Ph. Avouris, Nature (London) **398**, 299 (1999); H.R. Shea, R. Martel, Ph. Avouris, Phys. Rev. Lett. **84**, 4441 (2000)
22. M.F. Lin, D.S. Chuu, Phys. Rev. B **57**, 6731 (1998)
23. B.I. Dunlap, Phys. Rev. B **49**, 5643 (1994)
24. S.I. Chu, Adv. Chem. Phys. **73**, 739 (1989)
25. D.W. Hone, M. Holthaus, Phys. Rev. B **48**, 15123 (1993)
26. J.B. Krieger, G.J. Iafrate, Phys. Rev. B **33**, 5494 (1986)
27. J.P. Lu, Phys. Rev. Lett. **74**, 1123 (1995)
28. W. Deng, Y. Liu, C. Gong, Phys. Rev. B **50**, 7655 (1994)
29. J.W.G. Wildoer *et al.*, Nature **391**, 59 (1998)